



Variation in Eu^{3+} luminescence properties of $\text{GdF}_3:\text{Eu}^{3+}$ nanophosphors depending on matrix GdF_3 polytype

Xiaoting Zhang^{a,*}, Tomokatsu Hayakawa^a, Masayuki Nogami^a, Yukari Ishikawa^{a,b}

^a Ceramics Division, Department of Materials Science and Engineering, Nagoya Institute of Technology, Showa, Nagoya 466-8555, Japan

^b Japan Fine Ceramics Center, 2-4-1 Mutsumo, Atsuta, Nagoya 456-8587, Japan

ARTICLE INFO

Article history:

Received 30 August 2010

Received in revised form 13 October 2010

Accepted 28 October 2010

Available online 4 November 2010

Keywords:

Gadolinium trifluoride

Hexagonal

Orthorhombic

Rietveld method

Polytype

Luminescence

ABSTRACT

Hexagonal and orthorhombic $\text{GdF}_3:\text{Eu}^{3+}$ nanophosphors separately synthesized at room temperature were well characterized by X-ray diffraction (XRD) analysis and photoluminescence excitation and emission spectral measurements. Hexagonal $\text{GdF}_3:\text{Eu}^{3+}$ nanophosphors intrinsically exhibited stronger Eu^{3+} luminescence intensity under ultraviolet excitation. The Rietveld fitting of well-defined XRD data elucidated that the interatomic distances between Gd^{3+} ions in the hexagonal structure were shorter than those in the orthorhombic structure and that most Eu ions in $\text{GdF}_3:\text{Eu}^{3+}$ occupy Gd sites. The stronger luminescence in the hexagonal structure was conclusively explained by the much more efficient energy transfer from Gd to Eu in the hexagonal structure than in the orthorhombic structure, as determined on the basis of the interatomic distance between Gd and Eu.

© 2010 Elsevier B.V. All rights reserved.

1. Introduction

The lanthanide fluoride compounds LnF_3 and ALnF_4 (A = alkali metal, Ln = rare-earth element) have been widely used in many fields, such as optical telecommunication, lasers, new optoelectronic devices, diagnostics, and biological labels [1–5]. The polytype engineering of these materials has recently attracted attention. In fact, polytype NaYF_4 (or NaGdF_4) with hexagonal and cubic structures have been well documented [6–10]. However, studies of polytype LnF_3 , including GdF_3 , with hexagonal and orthorhombic structures are very few, most of which were focused on the phase transition mechanism at high temperatures [11–15]. Recently, stronger luminescence from Eu^{3+} in hexagonal EuF_3 than in orthorhombic EuF_3 has been reported [16]. This suggests that the polytype control of matrix LnF_3 makes it possible to increase the light-emitting probability of rare-earth-doped LnF_3 by the changing of atomic coordination around the doped rare earth.

Very recently, it has been demonstrated that $\text{GdF}_3:\text{Eu}^{3+}$ nanophosphors with hexagonal and orthorhombic structures can be individually prepared using different fluoride precursors at room temperature [17]. Hexagonal $\text{GdF}_3:\text{Eu}^{3+}$ “plate”-like nanocrystals (~100 nm) form with NaBF_4 as the fluoride precursor, while orthorhombic $\text{GdF}_3:\text{Eu}^{3+}$ “spindle”-like (300–400 nm in length and

60–100 nm in width) nanocrystals form with NH_4F as the fluoride precursor. It has also been pointed out that hexagonal $\text{GdF}_3:\text{Eu}^{3+}$ nanophosphors emit stronger luminescence than orthorhombic nanophosphors and the growth mechanism of GdF_3 nanocrystals has been discussed [17].

In the present work, our objective is to obtain reliable structural parameters via the Rietveld refinement procedure [18] using polytype $\text{GdF}_3:\text{Eu}^{3+}$ X-ray diffraction (XRD) patterns and to investigate the correlation between polytype and photoluminescence (PL) properties. PL properties were estimated by PL and photoluminescence excitation (PLE) spectral measurements as well as by a dynamic process of PL.

2. Experimental

All reagents were obtained from Aldrich Chem. Co. and used as received without further purification. Typical procedures for the synthesis of $\text{GdF}_3:\text{Eu}^{3+}$ nanocrystals are described as follows. First, 0.005 mol of $\text{Gd}(\text{NO}_3)_3 \cdot 6\text{H}_2\text{O}$ and 0.00025 mol of $\text{EuCl}_3 \cdot 6\text{H}_2\text{O}$ were dissolved in 100 ml of deionized water in a beaker at room temperature. After mechanical stirring for about 20 min, an aqueous solution of 0.015 mol of NaBF_4 (sample A) or 0.015 mol of NH_4F (sample B) was added dropwise. After constant stirring for 12 h at room temperature, a white precipitate was formed. Each precipitate was collected by three cycles of centrifugation and successive washing with water and ethanol. Subsequently, the final product was dried in an oven at 80 °C. The nominal Eu^{3+} concentration was fixed at 5 mol%. However the Eu^{3+} concentrations of sintered samples A and B were estimated to be 4% by energy-dispersive X-ray spectroscopy [17]. To study the change in the lattice parameter upon adding Eu^{3+} to GdF_3 , Eu-free GdF_3 polytype samples were also prepared by the same method. The Eu-free samples A and B are denoted as A⁰ and B⁰, respectively.

XRD analysis was performed on a Philips X'pert system using $\text{Cu K}\alpha$ radiation at a 45 kV voltage and a 40 mA current. The excitation and PL spectra were obtained

* Corresponding author.

E-mail address: chn13305@stn.nitech.ac.jp (X. Zhang).

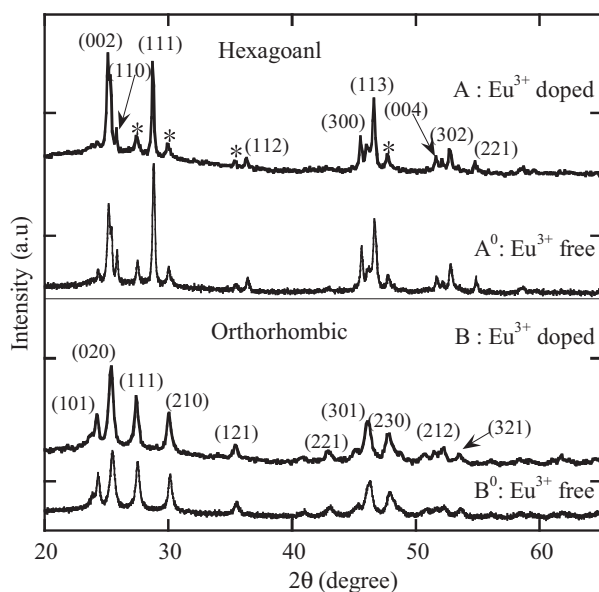


Fig. 1. XRD patterns of hexagonal (upper panel) and orthorhombic (lower panel) GdF_3 nanophosphors. Upper and lower patterns in a panel are Eu doped and Eu free, respectively.

using a F-7000 fluorescence spectrophotometer (Hitachi Co.). The PL decay curves of $^5\text{D}_0 \rightarrow ^7\text{F}_{1,2}$ transitions were recorded using a time-resolved fluorescence system (Oriol Instruments: InstaSpec™ V) under excitation with a 337.1 nm N_2 laser (Usho, KEC-200).

3. Results and discussion

Fig. 1 shows the X-ray powder diffraction patterns of samples A, A^0 , B, and B^0 . By comparison with those of hexagonal SmF_3 (PDF No. 05-0563), most of the diffraction peaks of samples A and A^0 were assigned to the hexagonal structure, although there are some minor residual orthorhombic structural peaks (marked with asterisks). For samples B and B^0 , all peaks were identified by comparison with the orthorhombic GdF_3 (PDF No. 12-0788) structure.

On the basis of the XRD patterns, the crystal structures of the prepared samples were refined by the Rietveld refinement using the software program RIETAN-FP (Izumi and Ikeda, 2000) [18]. For fitting, space groups of LnF_3 Pnma (D162h, No. 62) and P3-C1 (D43d, No. 165) [19] were used for samples A (A^0) and B (B^0), respectively.

In Table 1, the reported and fitted lattice parameters of LnF_3 materials are listed. The lattice parameters of LnF_3 linearly decreased in the sequence of SmF_3 , EuF_3 , GdF_3 , and TbF_3 , depending on the rare-earth ion radius in the orthorhombic structure. The lattice parameters a , b , and c of orthorhombic GdF_3 in this work ($a=0.6563$ nm, $b=0.6971$ nm, and $c=0.4387$ nm) were slightly smaller than the reported data ($a=0.6571$ nm, $b=0.6984$ nm, and

$c=0.439$ nm). Only the lattice parameters of hexagonal SmF_3 and EuF_3 are listed in Table 1, owing to the lack of data for hexagonal GdF_3 and TbF_3 in the JCPDS (Joint Committee for Powder Diffraction Standards) database. In hexagonal LnF_3 , a linear decrease in the lattice parameters with the rare-earth ion radius was also confirmed. The fitting results of samples A and B are shown in Fig. 2. The solid line and dots are the Rietveld fitting and observed XRD patterns, respectively. Comparing the Rietveld refinement results of Eu^{3+} -free and Eu^{3+} -doped samples, the lattice parameters of both Eu^{3+} -doped hexagonal and orthorhombic samples are slightly larger than those of the Eu^{3+} -free samples. As the valence and radius of the Gd ion were similar to those of the Eu ion, the replacement of Gd ion by the Eu ion doped into GdF_3 is reasonable. Taking account of the linear relation between the lattice parameters and the lanthanide ion radius, an expected increase in the lattice parameters can be calculated using

$$d_{\text{GdF}_3:\text{Eu}} = d_{\text{GdF}_3} + (d_{\text{GdF}_3} - d_{\text{EuF}_3})x \quad (1)$$

where

- $d_{\text{GdF}_3:\text{Eu}}$: lattice constant of $\text{GdF}_3:\text{Eu}$;
- d_{GdF_3} : lattice constant of GdF_3 ;
- d_{EuF_3} : lattice constant of EuF_3 ;
- x : Eu concentration in $\text{GdF}_3:\text{Eu}$.

In the case of 4% Eu doping, the increases in lattice parameters were $\Delta a_{\text{hc}}=0.17$ pm and $\Delta c_{\text{hc}}=0.10$ pm in hexagonal GdF_3 , and $\Delta a_{\text{oc}}=0.23$ pm, $\Delta b_{\text{oc}}=0.18$ pm and $\Delta c_{\text{oc}}=0.03$ pm in orthorhombic GdF_3 .

The measured values indicated that the increases in the lattice parameters upon 4% Eu doping in hexagonal GdF_3 were approximately $\Delta a_{\text{h}}=0.16$ pm and $\Delta c_{\text{h}}=0.18$ pm; and those in orthorhombic GdF_3 were approximately $\Delta a_0=0.23$ pm, $\Delta b_0=0.26$ pm and $\Delta c_0=0.56$ pm. The good consistency of the calculated increases in the lattice parameters with the measured values indicates that most Eu ions in GdF_3 can substitutionally be positioned at the Gd site.

On the basis of the Rietveld refinement results, crystal structures were drawn using VEST software and are shown in Fig. 3. In both the hexagonal and orthorhombic structures, the numbers of Gd^{3+} ions around the center Gd^{3+} ion are the same but the distances between Gd^{3+} ions are different as listed in Table 2. In the hexagonal structure, there are four equivalent nearest-neighbour Gd ion sites from the center Gd ion and the distance was calculated to be 0.38553 nm. On the other hand, there are two equivalent nearest-neighbour Gd ion sites from the center Gd site in the orthorhombic structure and the distance was 0.39307 nm. According to the Förster resonance energy transfer theory, the energy transfer probability is expressed

Table 1
Lattice parameters of LnF_3 .

Lattice parameter (nm)	SmF_3 (P63/mcm) (12-0792 ^a)	EuF_3 (p3-c1) (32-0373 ^a)	GdF (P3-c1) (this work A^0)	$\text{GdF}_3:\text{Eu}^{3+}$ (P3-c1) (this work A)		
Hexagonal						
$a=b$	0.6952	0.6920	0.687823 ± 0.000014	0.687979 ± 0.000022		
c	0.7122	0.7086	0.706216 ± 0.000025	0.706396 ± 0.000023		
Lattice parameter (nm)	SmF_3 (Pnma) (32-0981 ^a)	EuF_3 (Pnma) (33-0524 ^a)	GdF (Pnma) (49-1804 ^a)	GdF (Pnma) (this work B^0)	$\text{GdF}_3:\text{Eu}^{3+}$ (Pnma) (this work B)	TbF_3 (Pnma) (37-1487 ^a)
Orthorhombic						
a	0.6672	0.6620	0.6571	0.656308 ± 0.000016	0.656534 ± 0.000017	
b	0.7058	0.7015	0.684	0.697124 ± 0.000018	0.697388 ± 0.000028	
c	0.4404	0.4396	0.439	0.438739 ± 0.000011	0.439295 ± 0.000014	

^a JCPDS number.

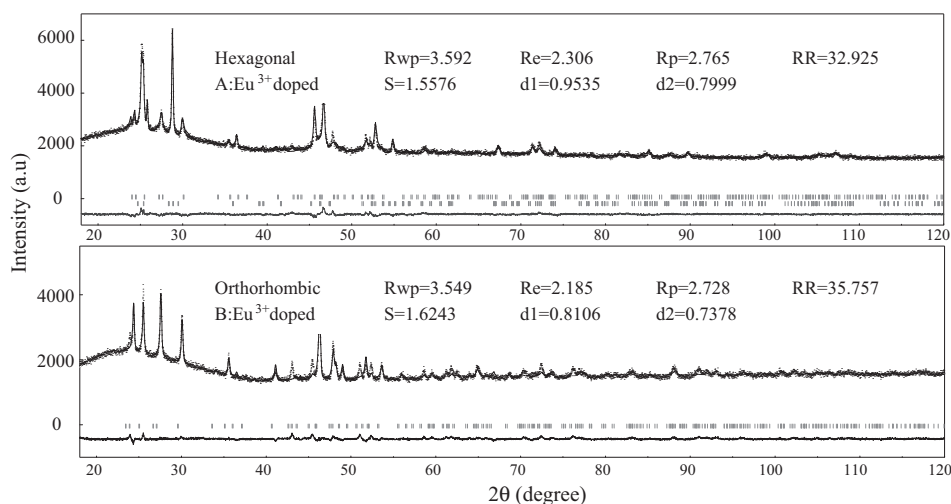


Fig. 2. Rietveld fitting profiles for polytypes of GdF_3 (sample A and B). Solid line and dots represent the calculated and measured profiles, respectively. The residual intensities are shown at the bottom of figure (jagged line), stick marks below the profile indicated the positions of the Bragg reflections.

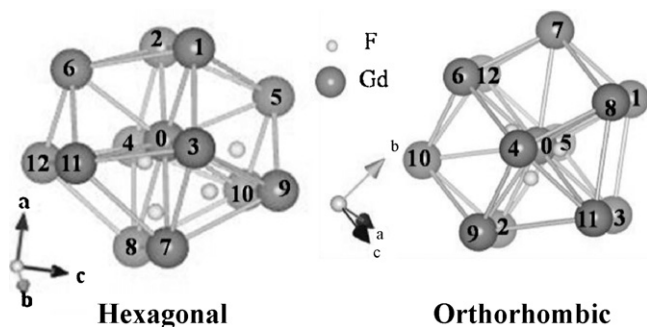


Fig. 3. Configuration of Gd^{3+} ions in hexagonal and orthorhombic $GdF_3:Eu^{3+}$ structure according to the Rietveld refinement results.

as follows [20,21]:

$$P_{AB} = \frac{1.4 \times 10^{24} f_A f_B S}{\Delta E^2 R^6}, \quad (2)$$

where

P_{AB} : probability of energy transfer,
 f_A, f_B : oscillator strengths of the donor and acceptor, respectively,
 S : overlap of donor emission and acceptor absorption,
 ΔE : transition energy,
 R : distance between the donor and acceptor.

Table 2

$Gd_x \rightarrow Gd_0$ distance in polytype $GdF_3:Eu^{3+}$. X denotes the ion site in Fig. 3.

X	Interatomic distance $Gd_x \rightarrow Gd_0$ (nm)	
	Hexagonal	Orthorhombic
1	0.385532	0.393070
2	0.385532	0.393070
3	0.385532	0.394006
4	0.385532	0.394006
5	0.406382	0.394006
6	0.406382	0.394006
7	0.421907	0.437152
8	0.421907	0.437152
9	0.421901	0.437152
10	0.421901	0.437152
11	0.421901	0.439695
12	0.421901	0.439695
Average	0.40959	0.41585

The probability of energy transfer depends inversely on the sixth power of the distance between the donor and the acceptor. Therefore, the shorter distance between Gd^{3+} and substituted Eu^{3+} ions in the hexagonal structure can induce a higher energy transfer probability from Gd^{3+} ions to Eu^{3+} ions than that in the orthorhombic structure.

The excitation spectra of 592 nm light emission from polytype $GdF_3:Eu^{3+}$ samples are shown in Fig. 4. The excitation peaks at 316 nm, 360 nm, 373 nm and 393 nm originate from the transitions from 7F_0 ground state to different excited states of Eu^{3+} , and the excitation peaks at 272 nm, 296 nm, 304 nm and 310 nm originate from the transitions of ${}^8S_{7/2} \rightarrow {}^6I_{7/2}$, ${}^8S_{7/2} \rightarrow {}^6P_{3/2}$, ${}^8S_{7/2} \rightarrow {}^6P_{5/2}$, and ${}^8S_{7/2} \rightarrow {}^6P_{7/2}$ of Gd^{3+} . Stronger excitation peaks at 272–310 nm based on the intratransition of Gd^{3+} than at 316–393 nm based on the intratransition of Eu^{3+} indicate that an efficient energy transfer from Gd^{3+} to Eu^{3+} in $GdF_3:Eu^{3+}$ occurs, as reported previously for $LiGdF_4:Eu^{3+}$ [22].

Fig. 5 shows the emission spectra of polytype $GdF_3:Eu^{3+}$ samples excited at 393 nm and 272 nm. They are dominated by the peaks located at 592 nm and 619 nm, corresponding to ${}^5D_0 \rightarrow {}^7F_1$ and ${}^5D_0 \rightarrow {}^7F_2$ transitions, respectively, in Eu^{3+} , which are typical magnetic and electronic dipole transitions [23]. Since the excitation of 272 nm corresponds to the transition ${}^8S_{7/2} \rightarrow {}^6I_7$ of Gd^{3+} , and 393 nm excitation corresponds to the transition ${}^7F_0 \rightarrow {}^5L_6$ of Eu^{3+} ions, it can be concluded that both the energy transfer from Gd^{3+} to Eu^{3+} and the intratransition in Eu^{3+} can excite PL (592 nm and 619 nm). Hexagonal $GdF_3:Eu^{3+}$ emitted a stronger luminescence

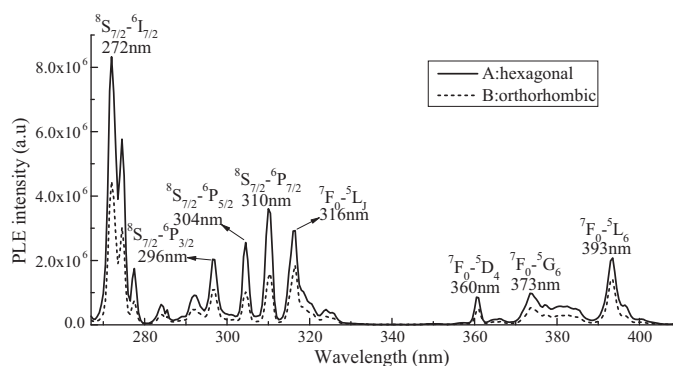


Fig. 4. Excitation spectra of hexagonal (solid line) and orthorhombic (dashed line) $GdF_3:Eu^{3+}$ nanophosphors at 592 nm.

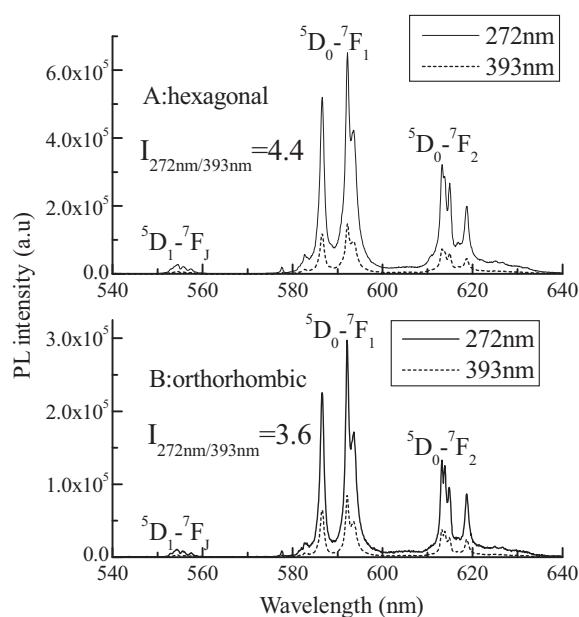


Fig. 5. Emission spectra of hexagonal (upper) and orthorhombic (lower) $\text{GdF}_3:\text{Eu}^{3+}$ nanophosphors excited at 272 nm and 396 nm.

than orthorhombic $\text{GdF}_3:\text{Eu}^{3+}$ under both excitation wavelengths. More remarkably, the luminescence intensity of the nanocrystals excited at 272 nm is in both cases stronger than that of the nanocrystals excited at 393 nm. The intensity ratio of the 592 nm emission peaks under different excitation at 272 nm and 393 nm was estimated to be 4.4 for the hexagonal structure. Similarly, the ratio of the 592 nm emission intensity at 272 nm and 393 nm excitation was estimated to be 3.6 for the orthorhombic structure. Therefore, the energy transfer probability from the Gd^{3+} ion to the Eu^{3+} ion in the hexagonal structure is higher than that in the orthorhombic structure if we assume that the absorption cross sections of the transition ${}^7\text{F}_0 \rightarrow {}^5\text{L}_6$ in Eu^{3+} ions are the same.

Fig. 6 shows the decay curves of ${}^5\text{D}_0 \rightarrow \text{F}_{1,2}$ emissions for polytype $\text{GdF}_3:\text{Eu}^{3+}$ nanophosphors. Luminescence decay curves can be well fitted with a double-exponential function using the least-squares fitting method:

$$\frac{I(t)}{I_0} = \alpha \exp\left(-\frac{t}{\tau_f}\right) + \beta \exp\left(-\frac{t}{\tau_s}\right) \quad (3)$$

where τ_f is the decay time of the fast component, τ_s is the decay time of the slow component, and α and β are the amplitude ratios of the fast and slow components, respectively ($\alpha + \beta = 1$) [17]. The results fitted to the decay curves are summarized in Table 3. For

Table 3

Lifetimes and amplitude ratio obtained by fitting the decay curves of ${}^5\text{D}_0 \rightarrow {}^7\text{F}_1$ and ${}^5\text{D}_0 \rightarrow {}^7\text{F}_2$ emission for $\text{GdF}_3:\text{Eu}^{3+}$ nanocrystals.

	${}^5\text{D}_0 \rightarrow {}^7\text{F}_1$ emission (592 nm)		${}^5\text{D}_0 \rightarrow {}^7\text{F}_2$ emission (619 nm)	
	Fast component	Slow component	Fast component	Slow component
Hexagonal $\text{GdF}_3:\text{Eu}^{3+}$ (A)	$\tau_f = 4.6$ ms $\alpha = 0.57$	$\tau_s = 14.97$ ms $\beta = 0.43$	$\tau_f = 1.84$ ms $\alpha = 0.36$	$\tau_s = 8.29$ ms $\beta = 0.64$
Orthorhombic $\text{GdF}_3:\text{Eu}^{3+}$ (B)	$\tau_f = 1.28$ ms $\alpha = 0.25$	$\tau_s = 7.06$ ms $\beta = 0.75$	$\tau_f = 4.6$ ms $\alpha = 0.4$	$\tau_s = 5.2$ ms $\beta = 0.6$

Table 4

Average lifetimes of Eu^{3+} ions ${}^5\text{D}_0 \rightarrow {}^7\text{F}_1$ and ${}^5\text{D}_0 \rightarrow {}^7\text{F}_2$ emission and fractional number located in higher symmetry sites in polytype GdF_3 nanocrystals.

	Average luminescence lifetime (ms)		Fraction of Eu^{3+} occupied symmetric site
	${}^5\text{D}_0 \rightarrow {}^7\text{F}_1$ (592 nm)	${}^5\text{D}_0 \rightarrow {}^7\text{F}_2$ (619 nm)	
Hexagonal $\text{GdF}_3:\text{Eu}^{3+}$ (A)	11.8	7.5	71%
Orthorhombic $\text{GdF}_3:\text{Eu}^{3+}$ (B)	6.7	4.8	69%

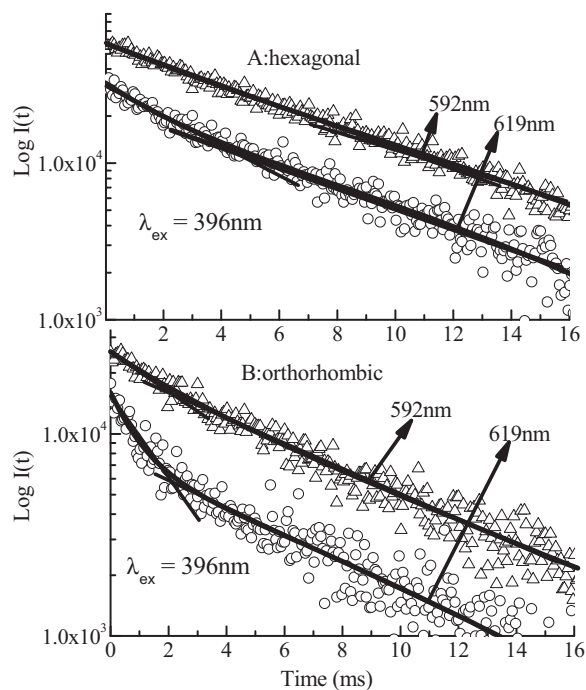


Fig. 6. Decay curves of ${}^5\text{D}_0 \rightarrow {}^7\text{F}_{1,2}$ emissions (592 and 619 nm) are shown by open triangles and open circles, respectively. The solid curves are fitting result to two exponential functions by a least-square fitting method. Left and right panels indicate hexagonal and orthorhombic $\text{GdF}_3:\text{Eu}^{3+}$ nanophosphors, respectively.

clarity, the average lifetimes of ${}^5\text{D}_0 \rightarrow {}^7\text{F}_{1,2}$ emissions were also calculated with Eq. (4) using the fitted results and are given in Table 4.

$$\tau = \frac{\alpha\tau_f^2 + \beta\tau_s^2}{\alpha\tau_f + \beta\tau_s} \quad (4)$$

It is very clear that hexagonal $\text{GdF}_3:\text{Eu}^{3+}$ exhibits a longer lifetime than orthorhombic $\text{GdF}_3:\text{Eu}^{3+}$, supporting the notion that Eu^{3+} ions are positioned in hexagonal systems with a higher symmetric structure.

As mentioned above, the ${}^5\text{D}_0 \rightarrow {}^7\text{F}_1$ emission peak at 592 nm from Eu^{3+} indicates a magnetic dipole transition in nature, which is insensitive to the atomic coordination around Eu^{3+} ions, however, the electric dipole transition of the ${}^5\text{D}_0 \rightarrow {}^7\text{F}_2$ peak at 619 nm from Eu^{3+} is quite sensitive to the atomic coordination. Since the atomic coordination around Eu^{3+} ions or the site symmetry of Eu^{3+} ions is strongly dependent on the location of Eu^{3+} in the GdF_3 matrix, that is, interstitial, surface-state, or substitutional Eu^{3+} in

GdF₃ nanocrystals, the decay behavior owing to electric-dipole and magnetic-dipole transitions includes information on the Eu location. The observed nonexponential decay curves (see Fig. 6), expressed by Eq. (3), mean that at least two sites for Eu³⁺ ions exist in GdF₃:Eu³⁺ nanocrystals for both hexagonal and orthorhombic structures. As previously reported [17], luminescence with a short lifetime can be observed from Eu³⁺ ions positioned in very asymmetric sites (e.g., surface-state and interstitial sites), whereas luminescence with a long lifetime was observed from Eu³⁺ ions in a highly-symmetric site. Considering the crystal structures of GdF₃, the latter site is considered to be a crystallographic position in the core of GdF₃ nanocrystals. The former must be a surface-state site or a position close to the surface of GdF₃ nanocrystals or interstitial site. Since $\alpha\tau_f$ and $\beta\tau_s$ are strongly correlated with the number of Eu³⁺ ions in the above-mentioned sites, the fractional numbers of Eu³⁺ ions positioned in the core of GdF₃ nanocrystals in both crystal systems can be estimated using the theory of transition probability and data obtained by decay curve analysis [24]. The results are listed in Table 4. The fractional numbers were 71% for the hexagonal structure and 69% for the orthorhombic structure. This estimation is strongly supported by the fact that from the results of Rietveld refinement, most Eu³⁺ ions could substitutionally be positioned at the Gd³⁺ site in hexagonal and orthorhombic GdF₃:Eu³⁺ nanocrystals. The similarity between the dispersibility of Eu³⁺ ions in the cores of hexagonal and orthorhombic GdF₃:Eu³⁺ nanocrystals indicates that the stronger Eu³⁺ luminescence of hexagonal GdF₃:Eu³⁺ nanocrystals is a consequence of the highly symmetric hexagonal structure and the shorter interatomic distance between Gd³⁺ and Eu³⁺ ions and, that the polytype structure is the main factor for determining the luminescence properties of these samples.

4. Conclusions

In this study, we succeeded in effectively characterizing hexagonal and orthorhombic GdF₃:Eu³⁺ nanophosphors synthesized by the precipitation method. It was estimated by the Rietveld fitting of XRD patterns and by PL dynamics analysis that most of the doped Eu replaced Gd in both polytypes. In addition, Rietveld analysis indicated that the interatomic distance between Gd and substituted Eu

in the hexagonal structure was shorter than that in the orthorhombic structure. A higher PL intensity owing to more efficient PL excitation via energy transfer from Gd³⁺ to Eu³⁺ in hexagonal GdF₃:Eu³⁺ nanophosphors was demonstrated. This was explained by the energy transfer probability, taking account of the interatomic distance. The polytype control (hexagonal–orthorhombic) of matrix LnF₃ enabled us to enhance the energy transfer probability from Gd³⁺ to Eu³⁺ by varying the interatomic distance.

References

- [1] B.M. Tissue, *Chem. Mater.* 10 (1998) 2837–2845.
- [2] Z.G. Chen, H.L. Chen, H. Hu, M.X. Yu, F.Y. Li, Q. Zhang, Z.G. Zhou, T. Yi, C.H. Huang, *J. Am. Chem. Soc.* 130 (2008) 3023–3029.
- [3] D.K. Chatterjee, A.J. Ruffal, Y. Zhang, *Biomaterials* 29 (2008) 937–943.
- [4] P.R. Diamente, M. Raudsepp, F.C.J.M. van Veggel, *Adv. Funct. Mater.* 17 (2007) 363–368.
- [5] S. Sivakumar, P.R. Diamente, F.C.J.M. van Veggel, *Chem. Eur. J.* 12 (2006) 5878–5884.
- [6] Z.J. Wang, F. Tao, L.Z. Yao, W.L. Cai, X.G. Li, *J. Cryst. Growth* 290 (2006) 196–300.
- [7] Z.L. Wang, J.H. Hao, H.L.W. Chan, *J. Mater. Chem.* 20 (2010) 3178–3185.
- [8] X.Q. Zhang, X.P. Fan, X.S. Qiao, Q. Luo, *Mater. Chem. Phys.* 121 (2010) 274–279.
- [9] M. Li, Z.-H. Hao, X.N. Peng, J.B. Li, X.F. Yu, Q.Q. Wang, *Opt. Express* 18 (2010) 3364–3369.
- [10] A. Mech, M. Karbowiak, L. Kepinski, A. Bednarkiewicz, W. Streck, *J. Alloys Compd.* 380 (2004) 315–320.
- [11] D.H. Allan Zalkin, *templeton, J. Am. Chem. Soc.* 75 (1953) 2453–2458.
- [12] R.E. Thoma, G.D. Brunton, *Inorg. Chem.* 5 (1966) 1937–1939.
- [13] K. Rotureau, Ph. Daniel, A. Desert, J.Y. Gesland, *J. Phys. Condens. Matter* 10 (1998) 1431–1446.
- [14] S.V. Stankus, R.A. Khairulin, K.M. Lyapunov, *J. Alloys Compd.* 290 (1999) 30–33.
- [15] C.H. Dong, M. Raudsepp, F.C.J.M. van Veggel, *J. Phys. Chem. C* 113 (2009) 472–478.
- [16] M. Wang, Q.L. Huang, J.M. Hong, X.T. Chen, Z.L. Xue, *Cryst. Growth Des.* 6 (2006) 1972–1974.
- [17] X.T. Zhang, T. Hayakawa, M. Nogami, Y. Ishikawa, *J. Nanomater.*, accepted.
- [18] F. Izumi, in: R.A. Young (Ed.), *The Rietveld Method*, Oxford University Press, 1993, Chapter 13.
- [19] *Handbook on the Physics and Chemistry of Rare Earths*, vol. 5, Elsevier North-Holland: Amsterdam, The Netherlands, 1982.
- [20] T. Förster, *Ann. Phys.* 55 (1948) 437.
- [21] R. Joseph, Lakowicz, *Principles of Fluorescence Spectroscopy*, 2nd ed., 1999.
- [22] R.T. Wegh, H. Donker, K.D. Oskam, A. Meijerink, *Science (Washington, DC, USA)* 283 (1999) 663.
- [23] W.T. Carnall, P.R. Fields, K. Rajnak, *J. Chem. Phys.* 49 (1968) 4450–4455.
- [24] X.T. Zhang, T. Hayakawa, M. Nogami, *J. Appl. Ceram. Tech. Int.* (in press).